ARTICLE

Light-Scattering Detection below the Level of Single Fluorescent Molecules for High-Resolution Characterization of Functional Nanoparticles

Shaobin Zhu,[†] Ling Ma,[†] Shuo Wang,[†] Chaoxiang Chen,[†] Wenqiang Zhang,[†] Lingling Yang,[†] Wei Hang,[†] John P. Nolan,[‡] Lina Wu,[†] and Xiaomei Yan*[,†]

[†]The MOE Key Laboratory of Spectrochemical Analysis & Instrumentation, The Key Laboratory for Chemical Biology of Fujian Province, Collaborative Innovation Center of Chemistry for Energy Materials, Department of Chemical Biology, College of Chemistry and Chemical Engineering, Xiamen University, Xiamen, Fujian 361005, People's Republic of China and [‡]The Scintillon Institute, 6404 Nancy Ridge Drive, San Diego, California 92121, United States

ABSTRACT Ultrasensitive detection and characterization of single nanoparticles (<100 nm) is important in nanotechnology and life sciences. Direct measurement of the elastically scattered light from individual nanoparticles represents the simplest and the most direct method for particle detection. However, the sixth-power dependence of scattering intensity on particle size renders very small particles indistinguishable from the background. Adopting strategies for single-molecule fluorescence detection in a sheathed flow, here we report the development of high sensitivity flow cytometry (HSFCM) that achieves real-time light-scattering detection of single silica and gold nanoparticles as small as 24 and 7 nm in diameter, respectively. This unprecedented sensitivity enables high-resolution sizing of single nanoparticles directly based on their scattered intensity. With a resolution comparable to that of TEM and the ease and speed of flow cytometric analysis, HSFCM is particularly suitable for nanoparticle size distribution analysis of polydisperse/heterogeneous/mixed samples. Through concurrent fluorescence detection, simultaneous insights into the size and payload variations of engineered nanoparticles are demonstrated with two forms of clinical nanomedicine. By offering quantitative multiparameter analysis of single nanoparticles in liquid suspensions at a throughput of up to 10 000 particles per minute, HSFCM represents a major advance both in light-scattering detection technology and in nanoparticle characterization.

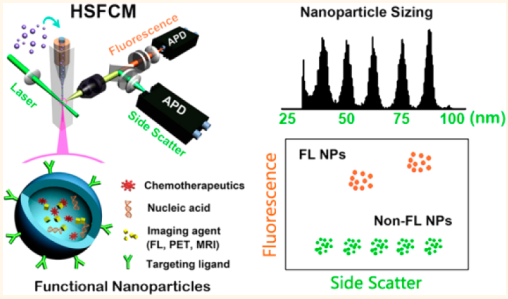

KEYWORDS: single-nanoparticle detection · light scattering · size distribution · nanomedicine · nanoparticle characterization · single-molecule detection · flow cytometry

Recent advances in nanotechnology offer exciting opportunities for the development of effective methods of disease diagnosis and treatment, as multiple imaging and therapeutic agents can be incorporated into nanoparticles (<100 nm) for targeted delivery.[1−5] Because these functional nanostructured materials are intrinsically heterogeneous, high-resolution physical and chemical characterization on a particle-by-particle basis is essential for successful clinical translation.[6−8] In addition to measurements of particle size and size distribution, biochemical properties such as the amount of therapeutic agent encapsulated or the number of targeting ligands conjugated to the surfaces of individual nanocarriers must be analyzed to achieve sufficient control for the synthesis of nanomedicines with consistent biological activities. However, the nanoscale dimensions and the limited number of cargo molecules encapsulated make single-nanoparticle characterization one of the biggest challenges in nanomedicine development.[6] Although single-particle techniques have progressed significantly in the detection, sizing, and counting of nanoparticles, simultaneous assessments of biochemical attributes are generally lacking.[9−15]

Flow cytometry (FCM) is a well-established technique for high-throughput, quantitative, and multiparameter analysis of individual cells and microscopic particles.[16−18] Information regarding particle size, shape, and

* Address correspondence to xmyan@xmu.edu.cn.

Received for review September 12, 2014 and accepted October 9, 2014.

Published online October 09, 2014
10.1021/nn505162u

morphology can be gathered *via* light scatter measurements, and biochemical attributes, such as the nucleic acid content, enzymatic activity, and antigenic determinant of biological cells, can be characterized *via* fluorescent labeling. However, it has been extremely difficult for conventional flow cytometry to detect particles smaller than 200 nm in diameter based on light scattering.[19] Great efforts have been made to detect single nanoparticles and viruses using custom-constructed flow cytometers,[20−24] and a 74 nm diameter polymer nanoparticle is the smallest particle that has been reliably detected based on scattering.[22]

Among optical techniques, elastic light scattering represents the simplest and most direct method of particle detection because it is label-free and applicable to all types of materials, including nonfluorescent and nonmetallic particles. Although single-molecule fluorescence detection has become routine in the laboratory, the light-scattering detection of single dielectric nanoparticles such as lipids, polymers, mesoporous silica, and virus-based drug delivery systems with sizes smaller than a few tens of nanometers remains a significant challenge. There are two major reasons for the difficulty of detecting such particles. First, according to the Rayleigh scattering theory, for spherical nanoparticles with sizes much smaller than the wavelength of the incident light, the intensity of the scattered light falls off with the sixth power of particle size, and the scattering cross section (σ_{scatt}) is given by[25]

$$\sigma_{scatt} = \frac{2\pi^5 d^6 n_{med}^4}{3\lambda^4}\left|\frac{m^2 - 1}{m^2 + 2}\right|^2 \quad (1)$$

where d is the particle diameter, λ is the wavelength of the incident light, n_{med} is the refractive index of the medium surrounding the particle, and m is the ratio of the refractive indices of the particle ($n_{particle} = n_{rel} + in_{im}$) and the medium ($n_{med}$). This strong size dependence renders the scattered light intensity of very small particles to rapidly vanish below the background noise. For example, the scattering cross section (σ_{scatt}) of a 25 nm diameter silica nanoparticle is only 0.0081 nm^2 at 532 nm, which is less than 1/3 of the absorption cross section (σ_{abs}) of a typical single-chromophore fluorescent dye such as fluorescein isothiocyanate (a molar extinction coefficient of 68 000 M^{-1} cm^{-1} corresponds to an absorption cross section of 0.026 nm^2). Second, the techniques that are employed to achieve single-molecule fluorescence detection, such as the spectrally filtered detection of Stokes-shifted fluorescence emission and the time-gated detection of delayed fluorescence photons for the rejection of spontaneously scattered light,[26] cannot be implemented to discriminate the elastically scattered light of a target particle against the scattering background from particle surroundings. In order to overcome the sixth-power scaling law of measuring the scattered intensity, interferometric techniques have been applied, in which the weak scattered field is combined with a reference field and the detected signal scales with the particle size to the third power as opposed to the sixth power.[9,12,27] Detection of single polystyrene nanoparticles of 30 nm in diameter and single gold nanoparticles below 10 nm in diameter has been demonstrated using interferometric measurements.[28,29]

In this study, we present the development of high-sensitivity flow cytometry (HSFCM) which demonstrates that light elastically scattered by single silica and gold nanoparticles as small as 24 and 7 nm in diameter, respectively, can be distinguished from the background *via* the direct measurement of the scattering intensity. This unprecedented sensitivity enables high-resolution nanoparticle sizing. Through concurrent fluorescence detection, quantitative multiparameter characterization of clinical nanomedicine is demonstrated through investigations of doxorubicin-encapsulated liposomes and small interfering RNA (siRNA)-loaded lipid nanoparticles.

RESULTS AND DISCUSSION

Apparatus and Detection Scheme. Our approach to the sensitive light-scattering detection of nanoparticles is inspired by strategies for single-molecule fluorescence detection in a sheathed flow, that is, a reduced probe volume for background reduction, an extended particle transit time for increased photon generation, and photon burst detection.[26,30] However, in our earlier instrument design, the single-photon counting avalanche photodiode (APD) detector used for fluorescence detection could not be applied for light-scattering detection of single nanoparticles due to the easy saturation of background scattering.[23] With PMT as the detector, the best signal-to-noise (S/N) ratio achieved for 100 nm diameter polystyrene beads was 104.[24] When the sixth-power dependence of light scattering on particle size is considered, significant sensitivity enhancement is required in order to detect dielectric nanoparticles as small as a few tens of nanometers in diameter. Figure 1a illustrates the schematic design of the current HSFCM system. In brief, a nanoparticle suspension is introduced into the center of a square-bore sheath-flow cuvette through a tapered quartz capillary (40 μm i.d.). The high-velocity sheath flow serves to hydrodynamically focus the sample flow into a very fine stream (~1.4 μm) that traverses the central region of the focused laser beam (~16 μm in diameter, unless stated otherwise), where the irradiation is most uniform. Therefore, each nanoparticle passes through the interrogating laser beam with the same velocity and experiences the same radiation field, thus providing foundation for the quantitative analysis of single nanoparticles. Perpendicular to the incident laser

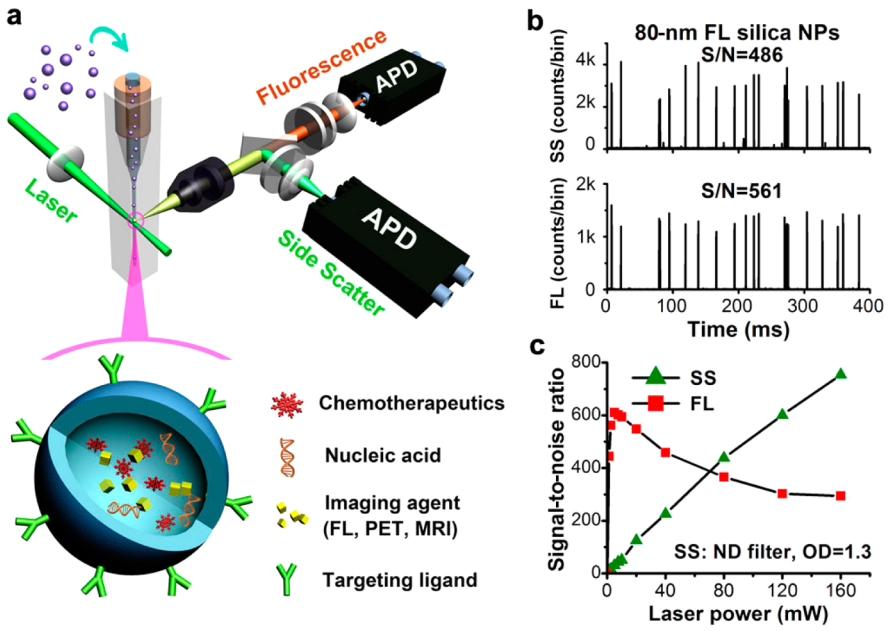

Figure 1. Laboratory-built HSFCM system and preliminary performance evaluation. (a) Schematic diagram of the laboratory-built apparatus and the structure of a nanomedicine. (b) Representative side-scatter and fluorescence (524/24 band pass) burst traces of 80 nm diameter fluorescent silica nanoparticles (425 MESF AF532) at a laser power of 16 mW, with a focused laser spot of 16 μm. (c) Effect of the laser power on the signal-to-noise ratios of the SS and FL detection of the 80 nm fluorescent silica nanoparticles. The focused laser spot was 6.4 μm, and a neutral density filter (OD = 1.3) was placed in the SS light path to avoid APD saturation.

beam and the flow of the sample, the emitted light from the sample stream is collected by an infinity-corrected microscope objective instead of the molded-glass Geltech aspheric lens and is then directed by a dichroic beam splitter into two light paths for side-scatter (SS) and fluorescence (FL) detection. In each light path, a focusing lens is used to project the image of the intersection of the laser beam and the sample stream onto an APD detector. The small active area (~180 μm in diameter) of the silicon APD detector serves as a limiting aperture to exclude laser light scattered from the cuvette windows and the sheath fluid. Details regarding the instrumentation setup and the data processing are provided in Supporting Information section 2.

Concurrent SS and FL detection was demonstrated through the analysis of 80 nm diameter fluorescent silica nanoparticles, the fluorescence intensity of which was calibrated to be 425 molecules of equivalent soluble fluorochrome (MESF) of Alexa Fluor 532 (AF532) (Figure 1b and Supporting Information Figure 1). Each nanoparticle passing through the interrogation volume produced a pulse or burst of photocurrent on both the SS and FL detection channels. For each burst, the integrated number of detected photons was recorded as the burst area. The S/N ratios, which were calculated as the average burst height of 3551 nanoparticles detected in 1 min divided by the standard deviation of the background signal (noise), were found to be 486 and 561 for SS and FL detection, respectively. The effects of the excitation laser power on both the SS and FL detection were studied. Whereas the S/N ratio of the fluorescence reached a maximum at approximately 5 mW and began to decrease thereafter because of fluorescence saturation, the detection sensitivity for light scattering continued to increase with increasing laser power (Figure 1c and Supporting Information Figure 2). These results suggest that a higher laser excitation energy density can be used to enhance the scattered light from single nanoparticles.

Light-Scattering Detection of Single Nanoparticles in the Low Nanometer Size Range. Employing the maximum laser power (160 mW) available to the current system and a focused laser spot of ~6.4 μm in diameter, the light-scattering detection of single nanoparticles was attempted for silica and gold nanoparticles in the low nanometer size range (Supporting Information section 1 and Figure 3). The representative burst-trace data presented in Figure 2a1 indicate that single silica nanoparticles of 29 nm in diameter (σ_{scatt} = 0.020 nm^2) could be detected with an S/N ratio of 27. The excellent discrimination of the signal from the background noise resulted in a well-defined SS burst-area distribution profile (Figure 2a2). An S/N ratio of 7 was achieved for the light-scattering detection of 24 nm diameter silica nanoparticles (σ_{scatt} = 0.0063 nm^2), although their light-producing power is equivalent to that of only 0.3 Alexa Fluor 532 molecules (Supporting Information section 3). On the other hand, due to the refractive index difference between silica (1.46) and polystyrene (1.59) at 532 nm in aqueous solution, a silica nanoparticle scatters approximately 4 times less light than

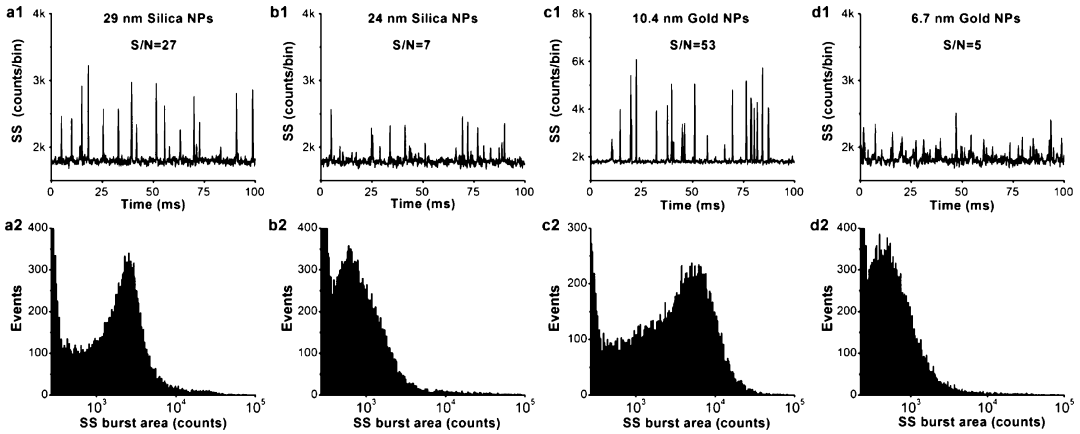

Figure 2. Light-scattering detection of single particles in the low nanometer range using HSFCM. (a−d) Representative SS burst traces (1) and burst-area distribution histograms (2) for 29 nm diameter silica nanoparticles (a), 14 nm diameter silica nanoparticles (b), 10.4 nm diameter gold nanoparticles (c), and 6.7 nm diameter gold nanoparticles (d). The laser excitation power was 160 mW, the focused laser spot was 6.4 μm, and no ND filter was placed in the SS light path. Each distribution histogram was derived from 1 min of data, and the nanoparticle concentrations were approximately 1−5 $\times$ 10^9/mL.

a polystyrene nanoparticle of the same size.[31] Therefore, pushing the detection limit for single dielectric nanoparticles from the previous state-of-the-art detection of ~75 nm diameter polystyrene nanoparticles[22] down to ~25 nm silica nanoparticles in the present study represents a gain of more than 3 orders of magnitude in sensitivity. To further demonstrate the sensitivity of the HSFCM system, gold nanoparticles of much smaller sizes were analyzed. Taking advantage of the localized surface plasmon resonance,[32] single gold nanoparticles as small as 10.4 and 6.7 nm in diameter were detected with S/N ratios of 53 (Figure 2c) and 5 (Figure 2d), respectively. We attribute the remarkable sensitivity of HSFCM in the light-scattering detection of single nanoparticles to the combined effects of (1) a further reduction of the detection volume down to ~10 fL by reducing the sample stream diameter and the focused laser beam spot size to minimize background emission, (2) a relatively long particle dwell time in the laser beam (~0.3 ms) and a relatively high laser excitation energy density (~5.0 $\times$ 10^5 W/cm^2 or ~1.3 $\times$ 10^{24} photons/s·cm^2) to generate more scattered photons (~2 $\times$ 10^4 for a 24 nm diameter silica nanoparticle), (3) the use of a single photon counting APD detector to achieve a high quantum efficiency of photon detection, and (4) an excellent optics to restrict the field-of-view of the APD detector solely to the sample stream for very good background rejection.

High-Resolution Sizing of Single Nanoparticles Based on the Scattered Light Intensity. By virtue of the exceptional sensitivity achieved in the light-scattering detection of single nanoparticles, we then examined the resolving power of HSFCM for the measurement of nanoparticle sizes by analyzing a mixture of monodisperse silica nanoparticles in five sizes ranging from 40 to 90 nm in diameter (Supporting Information Figure 4). To avoid APD saturation for large nanoparticles and to provide a more uniform radiation field in the sample fluid, a laser excitation power of 16 mW and a focused laser beam width of ~16 μm were used. A representative SS burst trace reveals that the peak heights clustered around five different amplitude levels, which corresponded to the five differently sized nanoparticle populations (Figure 3a). Because the particle analysis rate can approach 100−200 events per second, a statistically representative histogram of the SS burst-area distribution was obtained by rapidly interrogating thousands of nanoparticles individually at a time interval of 1 min, and baseline separation among the different populations was achieved (Figure 3b). It is worth noting that the dramatic (sixth-order) dependence of the light scattering on the particle size can be a double-edged sword. Once sufficient sensitivity is achieved, a 10% difference in particle diameter translates into an approximately 77% difference in light-scattering intensity, which yields high-resolution nanoparticle sizing.

When individual pure suspensions of silica nanoparticles of the five different sizes were measured *via* dynamic light scattering (DLS), significant overlap was observed in the compiled size distribution profiles (Figure 3d). When the centroids of the SS burst areas obtained from the fitted Gaussian curves (Figure 3b) were plotted as functions of the median diameters determined through transmission electron microscopy (TEM) for each nanoparticle population (Figure 3c), the resulting curve exhibited an approximately sixth-order dependence of intensity on particle size, in excellent agreement with the Rayleigh scattering theory (Figure 3e). Using this calibration curve, the particle size could be obtained by calculating the SS burst area, and the resultant size distribution profiles (Figure 3f) closely resembled those determined *via* TEM (Figure 3c). TEM is the technology that is most commonly used for the size and morphology characterization of nanoparticles, yet it cannot be operated

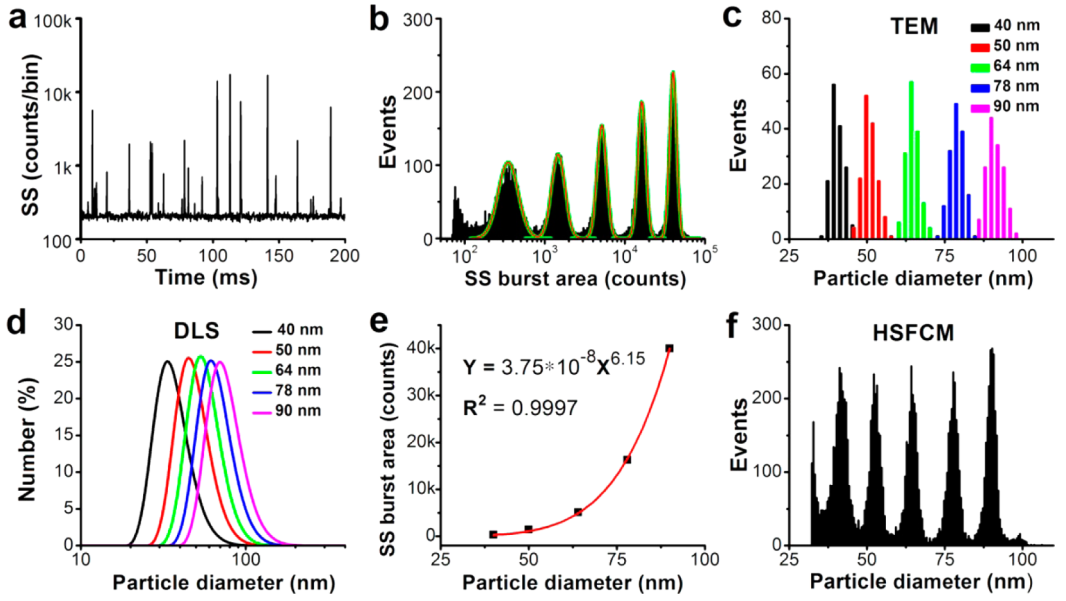

Figure 3. Comparison of HSFCM and conventional approaches for nanoparticle size distribution analysis. (a) Typical SS burst traces of a mixture of silica nanoparticles of five different sizes detected using the HSFCM. (b) SS burst-area distribution histogram derived from 1 min of data and the fit to a sum of Gaussian peaks. (c) Compiled particle size distribution histograms with a bin width of 2 nm for individual samples of five sizes of nanoparticles measured separately *via* TEM. (d) Compiled particle size distribution histograms (by particle number) for individual samples of five sizes of nanoparticles measured separately *via* DLS. (e) Plot of Gaussian-fitted SS burst areas as a function of the particle sizes determined *via* TEM. (f) Particle size distribution histogram with a bin width of 0.5 nm for the mixture of silica nanoparticles of five different sizes obtained using HSFCM.

under biologically relevant conditions and is of limited use in generating large population statistics. By offering rapid (with 1−2 min) and statistically reliable size distribution analyses of nanoparticles in liquid suspensions, HSFCM can serve as a complement to the TEM approach for the routine analysis and quality control of functional nanoparticles. One beneficial application of this technique could be the preclinical physicochemical characterization of a nanomedicine, including the measurement of its size distribution and its state of aggregation or agglomeration.

Simultaneous Particle Size and Drug Content Analysis of Doxorubicin-Carrying Liposomes. In nanomedicine development, nanoparticles are used as carriers to deliver payloads such as therapeutic agents; thus, the simultaneous detection of both nanoparticles and their cargos is desirable. Doxil (doxorubicin-carrying liposomes) is the first FDA-approved nanomedicine (1995), and DLS and cryo-TEM are the two most commonly used methods for size analysis.[33,34] To assess the feasibility of applying HSFCM for nanomedicine characterization, Doxoves, a research-grade product of PEGylated liposomal doxorubicin[35] whose physical characteristics and pharmacokinetics are comparable to those of Doxil, was analyzed as a model system. A representative cryo-TEM image and the particle size distribution histogram of Doxoves are provided in Figure 4a,b, respectively. A substantial amount of variation in both size and doxorubicin content can be observed among individual particles. The particle size, measured as the average of the long and short axes of the oval-shaped liposomes, was found to be 62 ± 11 nm. It is worth noting that when doxorubicin becomes crystallized inside liposomal particles, its fluorescence is quenched compared with that of the free drug in solution.[36] Despite the small particle size and the significant fluorescence quenching (~17-fold, Supporting Information Figure 5), Figure 4c demonstrates that HSFCM is sufficiently sensitive to detect both the scattered light and the intrinsic fluorescence of the doxorubicin emitted from each individual liposome. In as little as 1 min, more than 10 000 particles were analyzed, allowing statistically robust distributions to be rapidly generated (Figure 4d). Notably, particle size and drug content could be correlated at the single-particle level, and a positive correlation was identified.

Because of the comparable refractive indices of silica nanoparticles and lipid vesicles, monodisperse silica nanoparticles were used as the standard to calibrate the size measurement of the Doxoves nanoparticles based on their SS burst areas (Figure 4e), and a nicely distributed Gaussian profile was obtained within minutes (Figure 4f). The median size measured in this fashion is in good agreement with the results of the cryo-TEM measurement, and the distribution is more statistically representative. However, it is worth noting that, at a certain wavelength, the average refractive index of a liposome is determined by the refractive indices of its aqueous content and the lipids at the membrane (~1.48 at 488 nm) and by the volume

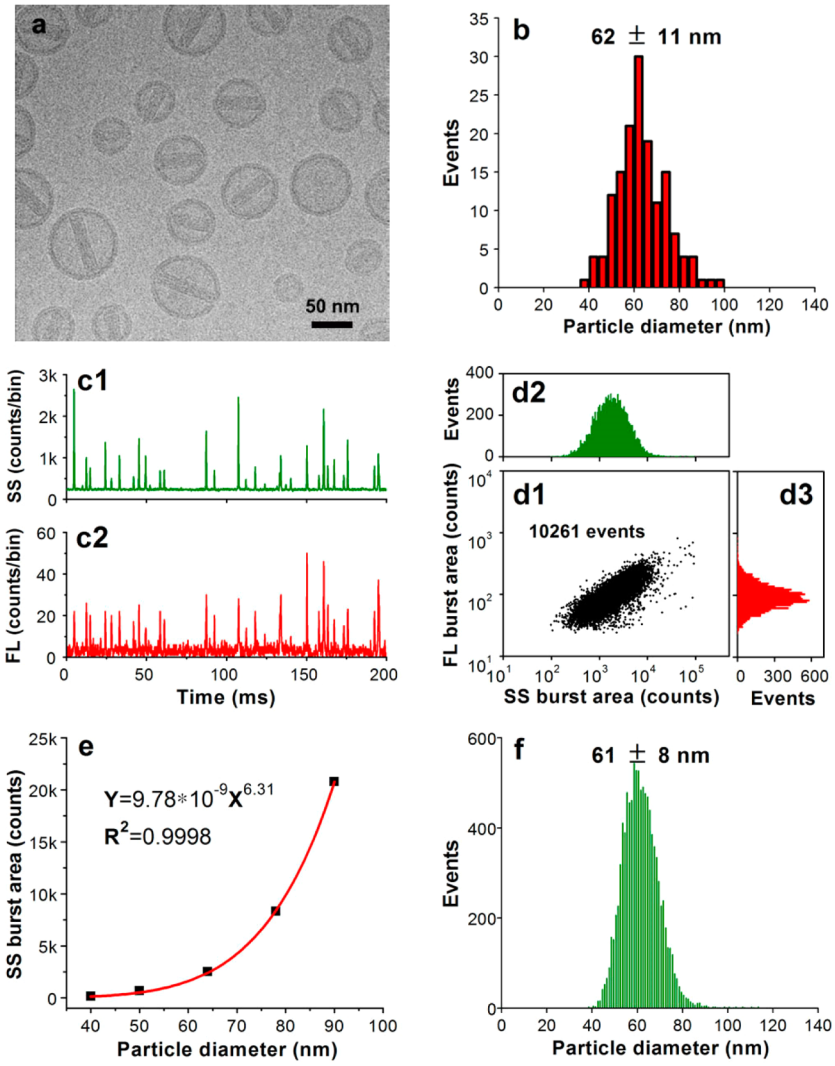

Figure 4. Characterization of doxorubicin-encapsulating liposomes. (a) Representative cryo-TEM image of Doxoves. (b) Particle size distribution histogram of Doxoves liposomes obtained from cryo-TEM images. (c) Representative SS and FL burst traces of Doxoves (diluted 4000-fold in 5% glucose) measured using HSFCM. (d) Bivariate dot-plot of the FL *versus* the SS burst area for Doxoves preparation. (e) Plot of nanoparticle SS burst area as a function of particle size for monodisperse silica nanoparticle standards. (f) Particle size distribution profile of Doxoves liposomes measured using HSFCM and the calibration curve presented in panel e.

fraction of lipids in the vesicle, in addition to the shape of the particle.[31,37,38] The encapsulation and crystallization of doxorubicin inside liposomes also complicates the issue. Therefore, caution must be taken if silica nanoparticles are to be used to accurately calibrate the size of liposomes with sizes or components different from Doxoves, as deviation from the true values may occur. Nevertheless, considering the very limited approaches that are available for the characterization of medicinal liposomes, HSFCM possesses a considerable advantage because it allows for the rapid and simultaneous analysis of size and drug content distributions at the single-particle level and in liquid suspensions.

Measurement of Particle Count and Fraction of siRNA Loading for Gene Delivery Systems. In addition to nanoparticle-based chemotherapy, nanoparticle-mediated gene therapy has received considerable attention over the past two decades.[39] Lipid nanoparticles (LNPs) encapsulating siRNA are currently the most extensively clinically validated means of enabling RNA interference.[40−42] However, it is challenging to determine the precise particle count and the fraction of loaded particles. Although, in principle, particles can be counted in cryo-TEM images, the nonuniformity of LNP distribution *in vitrified* samples on electron microscopy grids makes it difficult to obtain a precise particle count. Moreover, the comparable size, shape, and electron density of empty and siRNA-loaded LNPs render cryo-TEM less effective in determining the fraction of siRNA loading.[43]

We implemented HSFCM to characterize siRNA-loaded LNPs with the same composition as those currently being used in clinical testing.[44] The siRNA-loaded

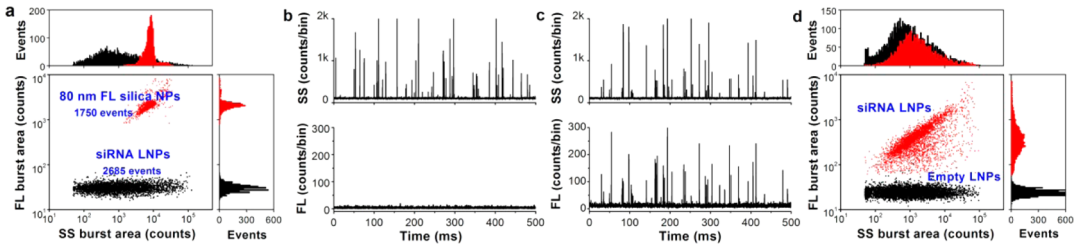

Figure 5. Characterization of siRNA nanomedicine using HSFCM. (a) Bivariate dot-plot of the FL burst area *versus* the SS burst area for a mixture of 80 nm diameter fluorescent nanoparticles with unstained siRNA-loaded LNPs. (b,c) Representative SS and FL burst traces for empty LNPs (b) and siRNA-loaded LNPs (c). (d) Compiled bivariate dot-plot of the FL burst area *versus* the SS burst area for empty and siRNA-loaded LNPs.

LNPs, along with empty LNPs as a control, were prepared by Alnylam Pharmaceuticals (Cambridge, MA). First, using an 80 nm diameter fluorescent silica nanoparticle of a known concentration as an internal standard, the particle concentration of siRNA-loaded LNPs (with an siRNA concentration of 0.1 mg/mL) was measured to be 7.0×10^{12} particles/mL (Figure 5a). Based on the concentration and molecular weight (~13 500 Da) of the encapsulated siRNA, it was calculated that the LNPs contained an average of ~650 siRNAs per particle. This single-particle enumeration approach is simple (label-free) and rapid (minutes), and it does not require a known mass density or the assumption of a regular shape.[45] Next, the empty and siRNA-loaded LNP samples were analyzed upon fluorescent staining with SYTO 82, a cell-permeant dye that labels nucleic acids. Figure 5b–d demonstrates that near-complete discrimination between the empty and siRNA-loaded LNPs was achieved based on the fluorescence signal, and the fraction of siRNA loading was determined to be approximately 100%. Through DLS measurement, the number-averaged sizes of the empty and siRNA-loaded LNPs were determined to be 45 ± 14 and 54 ± 13 nm, respectively. Therefore, the very broad distribution of the SS burst areas of the LNP specimens can most likely be attributed to the large intrinsic variation in particle size, which can be significantly exaggerated in the variation of the scattered light intensity because of the sixth-order dependence on particle size.

CONCLUSIONS

In summary, our study demonstrates for the first time that light-scattering detection of single nanoparticles with light-producing power below the level of single fluorescent molecules can be achieved by the HSFCM *via* the direct measurement of the scattering intensity. Most notably, adopting a sheathed flow system to confine the sample stream and isolate it far from the wall of the flow channel is indispensable to probe volume reduction and to the efficient block of the scattered light from cuvette windows. By pushing the light-scattering detection size limits for single nanoparticles down to 24 and 7 nm in diameter for silica and gold nanoparticles, respectively, HSFCM enables the analysis of nanoparticles that would have previously been difficult to characterize. Compared with other newly developed single-particle techniques, simultaneous assessments of various particle-associated biochemical attributes *via* current fluorescence detection represents a distinct advantage of the HSFCM. Our results extend the applicability and versatility of flow cytometry from the micron and submicron size range of particles down to the nanoscale. Besides the characterization of nanomedicines and other synthetic nanoparticles, we anticipate that HSFCM would open up new routes for the quantitative multiparameter analysis of naturally occurring biological nanoparticles, including viruses, cellular organelles, cell-derived exosomes, and protein assemblies.

METHODS

Transmission Electron Microscopy and Dynamic Light Scattering Measurements. TEM images of monodisperse silica nanoparticles and fluorescent silica nanoparticles were acquired using a JEOL JEM-2100 (HR) transmission electron microscope. Cryo-TEM measurement was performed using a Tecnai F20 transmission electron microscope (FEI) operating at 200 kV. The cryo-samples were prepared as follows: A special copper grid coated with carbon was processed through a Gatan SOLARUSTM plasma cleaning system to remove hydrocarbon contamination on the sample holder. Doxoves liposomal doxorubicin HCl was diluted 5-fold in 5% glucose buffer and then dropped onto the copper grid in the FEI Vitrobot sample plunger. The sample preparation was completed in the plunger. For each nanoparticle sample, 150 individual nanoparticles in the TEM micrographs were examined to determine the particle size distribution histogram and the median diameter. DLS measurements of nanoparticle samples were performed using a Zetasizer Nano-ZS90 (Malvern Instruments, Ltd.). A standard disposable cuvette was used to hold 100 μL of the nanoparticle suspension to be analyzed. Multiple measurements of each sample were averaged to improve accuracy. The mean and distribution were obtained in accordance with analysis by particle number.

Fluorescence Intensity Quantification of Fluorescent Silica Nanoparticles. The fluorescence intensity of the 80 nm diameter fluorescent silica nanoparticles was quantified in units of MESF per nanoparticle. Because the laser excitation wavelength was 532 nm and the Alexa Fluor family of fluorescent dyes are less pH sensitive and more photostable than the original dyes (*e.g.*, fluorescein, rhodamine), AF532 was used to calibrate the fluorescence intensity of silica nanoparticles doped with RBITC as

follows. A Shimadzu RF-5301 spectrofluorometer was used for the fluorescence measurement. AF532 solutions at selected concentrations were measured to construct a standard calibration curve. Then, the fluorescence signal of a 1.0×10^{11}/mL nanoparticle suspension (concentration calibrated against a diluted sample of a known concentration of 100 nm Orange FluoSpheres *via* single-particle enumeration using HSFCM) was compared with the calibration curve to determine the equivalent concentration of AF532 fluorochrome. The MESF-AF532 value per nanoparticle was then calculated by dividing the equivalent fluorochrome concentration by the particle concentration. The calibrated fluorescence intensity was found to be 425 MESF-AF532 for 80 nm diameter RBITC-doped fluorescent silica nanoparticles.

Fluorescence-Quenching Measurement of Liposome-Encapsulated Doxorubicin. One hundred microliters of Doxoves was applied to a Sephadex G-25 column and eluted with 3 mL of dilution buffer (10% sucrose, 10 mM histidine, pH = 6.5) to remove free doxorubicin. The liposome-encapsulated doxorubicin was released by treatment with 1% Triton X-100 at 65 °C for 15 min. The fluorescence-quenching factor of Doxoves was determined by measuring the fluorescence intensity before and after liposome disruption. In each case, the sample was diluted 64-fold to avoid fluorescence inner-filter effects resulting from a high particle concentration of Doxoves or a high concentration of released doxorubicin.

Staining of siRNA-Loaded Lipid Nanoparticles. Both the siRNA-loaded LNPs and the empty LNPs (approximately 1×10^{13}/mL) were diluted 4000-fold with DI water. SYTO 82 nucleic acid stain (at the stock concentration of 5 mM) was diluted 50-fold to 100 μM. Then, 2 μL of 100 μM SYTO 82 was added to 98 μL of each diluted LNP samples. The resulting mixture was incubated at 37 °C for 30 min prior to HSFCM analysis.

Conflict of Interest: The authors declare no competing financial interest.

Acknowledgment. This research was supported by the National Key Basic Research Program of China (Grant 2013CB933703), the National Natural Science Foundation of China (Grants 91313302, 21225523, 21027010, 20975087, and 90913015), the Program for Changjiang Scholars and Innovative Research Team in University (IRT13036), the National Fund for Fostering Talents of Basic Science (NFFTBS, Grant J1310024), the Fundamental Research Funds for the Xiamen University, and the U.S. NIH (R01 EB003824). The authors thank Z. Tian and B. Ren (Xiamen University) as well as A. Akinc (Alnylam Pharmaceuticals) for their suggestions. and thank G. Liang (University of Science and Technology of China) for assistance with the cryo-TEM analysis. We are grateful to Alnylam Pharmaceuticals (Cambridge, MA, USA) for providing the siRNA lipid nanoparticles.

Supporting Information Available: Materials and chemicals, high-sensitivity flow cytometry (HSFCM) instrumentation, and calculations. This material is available free of charge *via* the Internet at http://pubs.acs.org.

REFERENCES AND NOTES

1. Jain, R. K.; Stylianopoulos, T. Delivering Nanomedicine to Solid Tumors. *Nat. Rev. Clin. Oncol.* **2010**, *7*, 653–664.
2. Abeylath, S. C.; Ganta, S.; Iyer, A. K.; Amiji, M. Combinatorial-Designed Multifunctional Polymeric Nanosystems for Tumor-Targeted Therapeutic Delivery. *Acc. Chem. Res.* **2011**, *44*, 1009–1017.
3. Bourzac, K. Nanotechnology: Carrying Drugs. *Nature* **2012**, *491*, S58–S60.
4. Hubbell, J. A.; Langer, R. Translating Materials Design to the Clinic. *Nat. Mater.* **2013**, *12*, 963–966.
5. Chauhan, V. P.; Jain, R. K. Strategies for Advancing Cancer Nanomedicine. *Nat. Mater.* **2013**, *12*, 958–962.
6. Cressey, D. Tiny Traits Cause Big Headaches. *Nature* **2010**, *467*, 264–265.
7. Mullen, D. G.; Fang, M.; Desai, A.; Baker, J. R.; Orr, B. G.; Banaszak Holl, M. M. A Quantitative Assessment of Nanoparticle–Ligand Distributions: Implications for Targeted Drug and Imaging Delivery in Dendrimer Conjugates. *ACS Nano* **2010**, *4*, 657–670.
8. Grossman, J. H.; McNeil, S. E. Nanotechnology in Cancer Medicine. *Phys. Today* **2012**, *65*, 38–42.
9. Daaboul, G. G.; Yurt, A.; Zhang, X.; Hwang, G. M.; Goldberg, B. B.; Unlü, M. S. High-Throughput Detection and Sizing of Individual Low-Index Nanoparticles and Viruses for Pathogen Identification. *Nano Lett.* **2010**, *10*, 4727–4731.
10. Filipe, V.; Hawe, A.; Jiskoot, W. Critical Evaluation of Nanoparticle Tracking Analysis (NTA) by Nanosight for the Measurement of Nanoparticles and Protein Aggregates. *Pharm. Res.* **2010**, *27*, 796–810.
11. Gaiduk, A.; Yorulmaz, M.; Ruijgrok, P. V.; Orrit, M. Room-Temperature Detection of a Single Molecule's Absorption by Photothermal Contrast. *Science* **2010**, *330*, 353–356.
12. Mitra, A.; Deutsch, B.; Ignatovich, F.; Dykes, C.; Novotny, L. Nano-Optofluidic Detection of Single Viruses and Nanoparticles. *ACS Nano* **2010**, *4*, 1305–1312.
13. Wang, S.; Shan, X.; Patel, U.; Huang, X.; Lu, J.; Li, J.; Tao, N. Label-Free Imaging, Detection, and Mass Measurement of Single Viruses by Surface Plasmon Resonance. *Proc. Natl. Acad. Sci. U.S.A.* **2010**, *107*, 16028–16032.
14. Fraikin, J. L.; Teesalu, T.; McKenney, C. M.; Ruoslahti, E.; Cleland, A. N. A High-Throughput Label-Free Nanoparticle Analyser. *Nat. Nanotechnol.* **2011**, *6*, 308–313.
15. He, L.; Ozdemir, S. K.; Zhu, J.; Kim, W.; Yang, L. Detecting Single Viruses and Nanoparticles Using Whispering Gallery Microlasers. *Nat. Nanotechnol.* **2011**, *6*, 428–432.
16. Nantakomol, D.; Dondorp, A. M.; Krudsood, S.; Udomsangpetch, R.; Pattanapanyasat, K.; Combes, V.; Grau, G. E.; White, N. J.; Viriyavejakul, P.; Day, N. P.; *et al.* Circulating Red Cell-Derived Microparticles in Human Malaria. *J. Infect. Dis.* **2011**, *203*, 700–706.
17. Simons, P. C.; Young, S. M.; Carter, M. B.; Waller, A.; Zhai, D.; Reed, J. C.; Edwards, B. S.; Sklar, L. A. Simultaneous *In Vitro* Molecular Screening of Protein–Peptide Interactions by Flow Cytometry, Using Six Bcl-2 Family Proteins as Examples. *Nat. Protoc.* **2011**, *6*, 943–952.
18. Gregori, G.; Patsekin, V.; Rajwa, B.; Jones, J.; Ragheb, K.; Holdman, C.; Robinson, J. P. Hyperspectral Cytometry at the Single-Cell Level Using a 32-Channel Photodetector. *Cytometry, Part A* **2012**, *81*, 35–44.
19. van der Pol, E.; Coumans, F. A.; Grootemaat, A. E.; Gardiner, C.; Sargent, I. L.; Harrison, P.; Sturk, A.; van Leeuwen, T. G.; Nieuwland, R. Particle Size Distribution of Exosomes and Microvesicles Determined by Transmission Electron Microscopy, Flow Cytometry, Nanoparticle Tracking Analysis, and Resistive Pulse Sensing. *J. Thromb. Haemostasis* **2014**, *12*, 1182–1192.
20. Hercher, M.; Mueller, W.; Shapiro, H. M. Detection and Discrimination of Individual Viruses by Flow Cytometry. *J. Histochem. Cytochem.* **1979**, *27*, 350–352.
21. Zarrin, F.; Risfelt, J. A.; Dovichi, N. J. Light Scatter Detection within the Sheath Flow Cuvette for Size Determination of Multicomponent Submicrometer Particle Suspensions. *Anal. Chem.* **1987**, *59*, 850–854.
22. Steen, H. B. Flow Cytometer for Measurement of the Light Scattering of Viral and Other Submicroscopic Particles. *Cytometry, Part A* **2004**, *57*, 94–99.
23. Yang, L.; Zhu, S.; Hang, W.; Wu, L.; Yan, X. Development of an Ultrasensitive Dual-Channel Flow Cytometer for the Individual Analysis of Nanosized Particles and Biomolecules. *Anal. Chem.* **2009**, *81*, 2555–2563.
24. Zhu, S.; Wang, S.; Yang, L.; Huang, T.; Yan, X. Progress in the Development of Techniques Based on Light Scattering for Single Nanoparticle Detection. *Sci. China: Chem.* **2011**, *54*, 1244–1253.
25. Bohren, C. F.; Huffman, D. R. *Absorption and Scattering of Light by Small Particles*; John Wiley & Sons: New York, 1983.
26. Keller, R. A.; Ambrose, W. P.; Goodwin, P. M.; Jett, J. H.; Martin, J. C.; Wu, M. Single-Molecule Fluorescence Analysis in Solution. *Appl. Spectrosc.* **1996**, *50*, 12A–32A.
27. Kukura, P.; Ewers, H.; Muller, C.; Renn, A.; Helenius, A.; Sandoghdar, V. High-Speed Nanoscopic Tracking of the Position and Orientation of a Single Virus. *Nat. Methods* **2009**, *6*, 923–927.

28. Lindfors, K.; Kalkbrenner, T.; Stoller, P.; Sandoghdar, V. Detection and Spectroscopy of Gold Nanoparticles Using Supercontinuum White Light Confocal Microscopy. *Phys. Rev. Lett.* **2004**, *93*, 037401.
29. Ignatovich, F. V.; Novotny, L. Real-Time and Background-Free Detection of Nanoscale Particles. *Phys. Rev. Lett.* **2006**, *96*, 013901.
30. Ambrose, W. P.; Goodwin, P. M.; Jett, J. H.; Van Orden, A.; Werner, J. H.; Keller, R. A. Single Molecule Fluorescence Spectroscopy at Ambient Temperature. *Chem. Rev.* **1999**, *99*, 2929–2956.
31. Chandler, W. L.; Yeung, W.; Tait, J. F. A New Microparticle Size Calibration Standard for Use in Measuring Smaller Microparticles Using a New Flow Cytometer. *J. Thromb. Haemostasis* **2011**, *9*, 1216–1224.
32. Anker, J. N.; Hall, W. P.; Lyandres, O.; Shah, N. C.; Zhao, J.; Van Duyne, R. P. Biosensing with Plasmonic Nanosensors. *Nat. Mater.* **2008**, *7*, 442–453.
33. Lengyel, J. S.; Milne, J. L.; Subramaniam, S. Electron Tomography in Nanoparticle Imaging and Analysis. *Nanomedicine* **2008**, *3*, 125–131.
34. Barenholz, Y. Doxil(R): The First FDA-Approved Nano-Drug: Lessons Learned. *J. Controlled Release* **2012**, *160*, 117–134.
35. http://www.liposomeexpert.com/categories/drug-loaded-liposomes/.
36. Zhao, Y.; Alakhova, D. Y.; Kim, J. O.; Bronich, T. K.; Kabanov, A. V. A Simple Way To Enhance Doxil(R) Therapy: Drug Release from Liposomes at the Tumor Site by Amphiphilic Block Copolymer. *J. Controlled Release* **2013**, *168*, 61–69.
37. Matsuzaki, K.; Murase, O.; Sugishita, K.; Yoneyama, S.; Akada, K.; Ueha, M.; Nakamura, A.; Kobayashi, S. Optical Characterization of Liposomes by Right Angle Light Scattering and Turbidity Measurement. *Biochim. Biophys. Acta* **2000**, *1467*, 219–226.
38. van der Pol, E.; van Gemert, M. J.; Sturk, A.; Nieuwland, R.; van Leeuwen, T. G. Single *vs*. Swarm Detection of Microparticles and Exosomes by Flow Cytometry. *J. Thromb. Haemostasis* **2012**, *10*, 919–930.
39. Seymour, L. W.; Thrasher, A. J. Gene Therapy Matures in the Clinic. *Nat. Biotechnol.* **2012**, *30*, 588–593.
40. Zimmermann, T. S.; Lee, A. C.; Akinc, A.; Bramlage, B.; Bumcrot, D.; Fedoruk, M. N.; Harborth, J.; Heyes, J. A.; Jeffs, L. B.; John, M.; *et al.* RNAi-Mediated Gene Silencing in Non-human Primates. *Nature* **2006**, *441*, 111–114.
41. Whitehead, K. A.; Langer, R.; Anderson, D. G. Knocking down Barriers: Advances in SiRNA Delivery. *Nat. Rev. Drug Discovery* **2009**, *8*, 129–138.
42. Semple, S. C.; Akinc, A.; Chen, J.; Sandhu, A. P.; Mui, B. L.; Cho, C. K.; Sah, D. W.; Stebbing, D.; Crosley, E. J.; Yaworski, E.; *et al.* Rational Design of Cationic Lipids for SiRNA Delivery. *Nat. Biotechnol.* **2010**, *28*, 172–176.
43. Leung, A. K.; Hafez, I. M.; Baoukina, S.; Belliveau, N. M.; Zhigaltsev, I. V.; Afshinmanesh, E.; Tieleman, D. P.; Hansen, C. L.; Hope, M. J.; Cullis, P. R. Lipid Nanoparticles Containing SiRNA Synthesized by Microfluidic Mixing Exhibit an Electron-Dense Nanostructured Core. *J. Phys. Chem. C* **2012**, *116*, 18440–18450.
44. Jayaraman, M.; Ansell, S. M.; Mui, B. L.; Tam, Y. K.; Chen, J.; Du, X.; Butler, D.; Eltepu, L.; Matsuda, S.; Narayanannair, J. K.; *et al.* Maximizing the Potency of SiRNA Lipid Nanoparticles for Hepatic Gene Silencing *in Vivo*. *Angew. Chem., Int. Ed.* **2012**, *51*, 8529–8533.
45. Zhu, S.; Yang, L.; Long, Y.; Gao, M.; Huang, T.; Hang, W.; Yan, X. Size Differentiation and Absolute Quantification of Gold Nanoparticles *via* Single Particle Detection with a Laboratory-Built High-Sensitivity Flow Cytometer. *J. Am. Chem. Soc.* **2010**, *132*, 12176–12178.